Array of tapered semiconductor waveguides in a fiber for infrared image transfer and magnification

M. Krishnamurthi,[1] J. R. Sparks,[2] R. He,[2] I. A. Temnykh,[1] N. F. Baril,[2] Z. Liu,[3] P. J. A. Sazio,[4] J. V. Badding,[2] and V. Gopalan[1,*]

[1]*Department of Material Science and Engineering, The Pennsylvania State University, University Park, Pennsylvania 16802, USA*

[2]*Department of Chemistry, The Pennsylvania State University, University Park, Pennsylvania 16802, USA*

[3]*Department of Electrical Engineering, The Pennsylvania State University, University Park, Pennsylvania 16802, USA*

[4]*Optoelectronics Research Center, University of Southampton, Southampton, SO17 1BJ, UK*

[*]*vgopalan@psu.edu*

Abstract: The proof-of-concept of an infrared imaging tip by an array of infrared waveguides tapered as small as 2 μm is demonstrated. The fabrication is based on a high-pressure chemical fluid deposition technique to deposit precisely defined periodic arrays of Ge and Si waveguides within a microstructured optical fiber template made of silica to demonstrate the proposed concept at wavelengths of 10.64 μm and 1.55 μm, respectively. The essential features of the imaging system such as isolation between adjacent pixels, magnification, optical throughput, and image transfer characteristics are investigated. Near-field scanning at 3.39 μm wavelength using a single tapered Ge core is also demonstrated.

OCIS codes: (110.2350) Fiber optics imaging; (110.3080) Infrared imaging; (160.1245) Artificially engineered materials; (160.2290) Fiber materials.

References and links

1. Y. C. Shen, T. Lo, P. F. Taday, B. E. Cole, W. R. Tribe, and M. C. Kemp, "Detection and identification of explosives using terahertz pulsed spectroscopic imaging," Appl. Phys. Lett. **86**(24), 241116 (2005).
2. R. Mendelsohn, E. P. Paschalis, P. J. Sherman, and A. L. Boskey, "IR microscopic imaging of pathological states and fracture healing of bone," Appl. Spectrosc. **54**(8), 1183–1191 (2000).
3. B. T. Soifer, G. Neugebauer, K. Matthews, E. Egami, E. E. Becklin, A. J. Weinberger, M. Ressler, M. W. Werner, A. S. Evans, N. Z. Scoville, J. A. Surace, and J. J. Condon, "High resolution mid-infrared imaging of ultraluminous infrared galaxies," Astron. J. **119**(2), 509–523 (2000).
4. J. F. Head and R. L. Elliott, "Infrared imaging: making progress in fulfilling its medical promise," IEEE Eng. Med. Biol. Mag. **21**(6), 80–85 (2002).
5. D. J. Titman, "Applications of thermography in non-destructive testing of structures," NDT Int. **34**(2), 149–154 (2001).
6. G. Reich, "Near-infrared spectroscopy and imaging: basic principles and pharmaceutical applications," Adv. Drug Deliv. Rev. **57**(8), 1109–1143 (2005).
7. L. P. Ghislain, V. B. Elings, K. B. Crozier, S. R. Manalis, S. C. Minne, K. Wilder, G. S. Kino, and C. F. Quate, "Near-field photolithography with a solid immersion lens," Appl. Phys. Lett. **74**(4), 501–503 (1999).
8. C. A. Michaels, "Mid-infrared imaging with a solid immersion lens and broadband laser source," Appl. Phys. Lett. **90**(12), 121131 (2007).
9. D. A. Fletcher, K. B. Crozier, K. W. Guarini, S. C. Minne, G. S. Kino, C. F. Quate, and K. E. Goodson, "Microfabricated silicon solid immersion lens," J. Microelectromech. Syst. **10**(3), 450–459 (2001).
10. M. Shinoda, K. Saito, T. Ishimoto, T. Kondo, A. Nakaoki, N. Ide, M. Furuki, M. Takeda, Y. Akiyama, T. Shimouma, and M. Yamamoto, "High-density near-field optical disc recording," Jpn. J. Appl. Phys. **44**(5B), 3537–3541 (2005).
11. Y. Kim, J. Zhang, and T. D. Milster, "GaP solid immersion lens based on diffraction," Jpn. J. Appl. Phys. **48**(3), 03A047 (2009).
12. K. B. Cozier, D. A. Fletcher, G. S. Kino, C. F. Quate, and H. T. Soh, "Near field optical scanning system employing microfabricated solid immersion lens," US Patent 6441359 (2002).

#160359 - $15.00 USD Received 21 Dec 2011; accepted 24 Jan 2012; published 3 Feb 2012

13. F. Huth, M. Schnell, J. Wittborn, N. Ocelic, and R. Hillenbrand, "Infrared-spectroscopic nanoimaging with a thermal source," Nat. Mater. **10**(5), 352–356 (2011).
14. M. M. Qazilbash, M. Brehm, G. O. Andreev, A. Frenzel, P. C. Ho, B.-G. Chae, B.-J. Kim, S. Yun, H.-T. Kim, A. Balatsky, O. Shpyrko, M. Maple, F. Keilmann, and D. Basov, "Infrared spectroscopy and nano-imaging of the insulator-to-metal transition in vanadium dioxide," Phys. Rev. B **79**(7), 075107 (2009).
15. I. Gannot, A. Goren, E. Rave, A. Katzier, V. Gopal, G. Revezin, and J. A. Harrington, "Thermal imaging through infrared fiber/waveguides bundles," Proc. SPIE **5317**, 95 (2004).
16. U. Gal, J. Harrington, M. Ben-David, C. Bledt, N. Syzonenko, and I. Gannot, "Coherent hollow-core waveguide bundles for thermal imaging," Appl. Opt. **49**(25), 4700–4709 (2010).
17. G. Shvets, S. Trendafilov, J. B. Pendry, and A. Sarychev, "Guiding, focusing, and sensing on the subwavelength scale using metallic wire arrays," Phys. Rev. Lett. **99**(5), 053903 (2007).
18. S. Kawata, A. Ono, and P. Verma, "Subwavelength colour imaging with a metallic nanolens," Nat. Photonics **2**(7), 438–442 (2008).
19. P. J. A. Sazio, A. Amezcua-Correa, C. E. Finlayson, J. R. Hayes, T. J. Scheidemantel, N. F. Baril, B. R. Jackson, D. J. Won, F. Zhang, E. R. Margine, V. Gopalan, V. H. Crespi, and J. V. Badding, "Microstructured optical fibers as high-pressure microfluidic reactors," Science **311**(5767), 1583–1586 (2006).
20. E. Palik, *Handbook of Optical Constants of Solids II* (Academic Press, New York 1998).
21. P. Mehta, M. Krishnamurthi, N. Healy, N. F. Baril, J. R. Sparks, P. J. A. Sazio, V. Gopalan, J. V. Badding, and A. C. Peacock, "Mid-infrared transmission properties of amorphous germanium optical fibers," Appl. Phys. Lett. **97**(7), 071117 (2010).
22. N. F. Baril, B. Keshavarzi, J. R. Sparks, M. Krishnamurthi, I. A. Temnykh, P. J. A. Sazio, A. C. Peacock, A. Borhan, V. Gopalan, and J. V. Badding, "High-pressure chemical deposition for void-free filling of extreme aspect ratio templates," Adv. Mater. (Deerfield Beach Fla.) **22**(41), 4605–4611 (2010).
23. N. Healy, J. R. Sparks, P. J. A. Sazio, J. V. Badding, and A. C. Peacock, "Tapered silicon optical fibers," Opt. Express **18**(8), 7596–7601 (2010).
24. L. Lagonigro, N. Healy, J. R. Sparks, N. F. Baril, P. J. A. Sazio, J. V. Badding, and A. C. Peacock, "Low loss silicon fibres for photonics applications," Appl. Phys. Lett. **96**(4), 041105 (2010).
25. J. R. Sparks, R. He, N. Healy, M. Krishnamurthi, A. C. Peacock, P. J. A. Sazio, V. Gopalan, and J. V. Badding, "Zinc selenide optical fibers," Adv. Mater. (Deerfield Beach Fla.) **23**(14), 1647–1651 (2011).

1. Introduction

Infrared imaging with high resolution is of increasing importance in research areas such as chemical sensing, biomedical diagnosis, thermography, non-destructive testing and astronomy [1–6]. Contemporary high-resolution infrared imaging tools are based either on solid immersion lenses (SIL) or near-field scanning techniques, or a combination of both [7–12]. The SIL offers diffraction limited imaging over larger areas with high optical throughput, while near-field technique offers excellent resolution beyond the diffraction limit [13, 14], but with low optical throughput and longer acquisition times. For far-field infrared imaging, flexible fiber-optic bundle endoscopes are a preferred technique for rapid imaging of specimens with restricted optical access in a minimally invasive manner [15]. The incumbent technology for infrared imaging between 2 to 10 μm wavelengths using coherent fiber-optic bundles is based on arrays of either hollow metallic or chalcogenide core waveguides. These imaging bundles operate over a broad wavelength range, but have been limited to modest pixel sizes of the order of 50-100 μm [16]. Other plasmonics based techniques have been proposed, which can offer high resolution, but also high optical losses [17, 18]. Therefore, there is a need for low-loss, broadband imaging systems with high resolution at mid-infrared wavelengths. Here we present the conceptual design, fabrication scheme, and optical characterization of an imaging system based on deposited semiconductor waveguides in tapered microstructured optical fibers (MOFs). The transfer of an image with magnification across the tip is also demonstrated. Although continuous broadband imaging is not demonstrated, imaging at two specific wavelengths of 10.6 μm and 3.39 μm is demonstrated. Near-field scanning at 3.39 μm wavelength is also demonstrated.

The conceptual imaging fiber structure is illustrated in Fig. 1(a). Since the technology used for fabricating MOFs such as in Fig. 1(b) is already well developed, the spatial arrangement and diameters of the pores can be precisely engineered. Each tapered waveguide deposited via a high-pressure chemical fluid deposition technique [19] within a pore operates as a pixel in the imaging system. The resolution is determined by the diameter of the individual waveguides (pixels) that are tapered down to have sub-wavelength dimensions at the input, as

#160359 - $15.00 USD Received 21 Dec 2011; accepted 24 Jan 2012; published 3 Feb 2012

well as the pitch between the pixels. In such a conceptual design, a magnified image will be transmitted from the input (narrow) end with sub-wavelength pixel and pitch sizes to the un-tapered (wider) output end of the MOF as shown in the finite element simulation of Fig. 1(c). Therefore, potentially, thousands of such waveguides can be densely packed, and can aid in the transport and confinement of photons from the object to the image plane.

For demonstrating proof-of-concept infrared imaging with sub-wavelength pixel size, an array of tapered germanium (Ge) waveguides was fabricated and characterized. Ge has a broad transmission window ranging from 2 to 15 μm [20]. For wavelengths below 2 μm, a similar structure with an array of silicon (Si) waveguides was also fabricated. Another inherent advantage of this design is the strongly infrared (>2.5 μm) absorbing silica matrix that will assist in the reduction of cross-talk between pixels. A natural limitation of an array of waveguides is that larger overall tip size of the array will limit imaging to only planar samples. A single Ge pixel taper was also fabricated and near-field imaging resolution is demonstrated. Since the near-field is reasonably considered to be on the order of ~λ/10, the tip-sample separation for IR imaging will be on the order of 0.3-1 μm for wavelengths of λ = 3-10 μm.

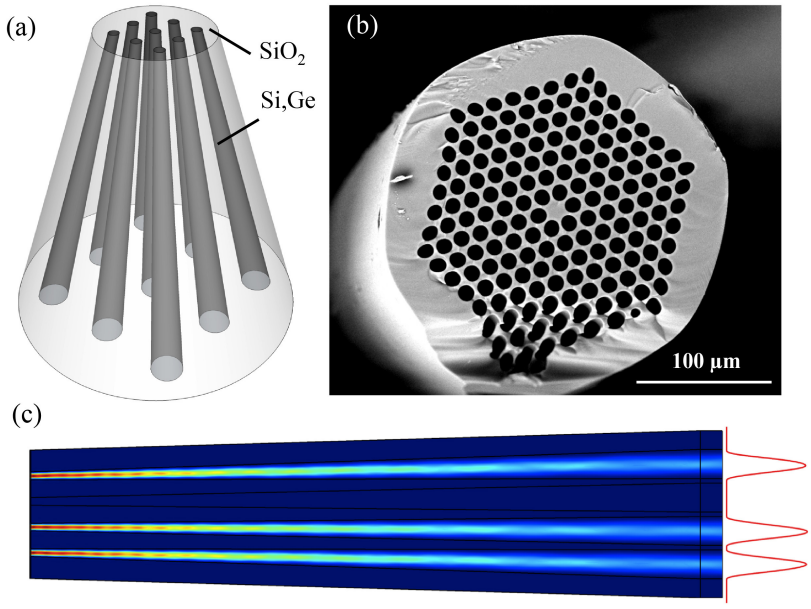

Fig. 1. (a) Schematic of the proposed tapered fiber design. (b) Scanning electron micrograph of a silica based microstructured optical fiber used as a template for fabricating the proposed structure. (c) A two-dimensional COMSOL™ simulation of four 300 μm long tapered Ge waveguides (3.5/13 μm input/output diameters, pitch of 11.5/15 μm at the input and output facets). A metal mask (modeled as perfect conductor) at the input left end covers the input end except for three of the Ge waveguides. Plane waves at λ = 10.6 μm are launched at the narrow input end and detected at the broader output end. Cross-talk between the pixels is <1%, as calculated from the ratio of the transmitted intensities from the blocked pixel to that from a transmitting pixel.

2. Fabrication

To fabricate the desired tapered waveguide structures, the chemical fluid deposition processing parameters for fabricating a single tapered Ge/Si waveguide within a silica capillary were first determined [19,21–23] and then extended to fabricate an array of tapered waveguides. Tapered waveguides can be fabricated by either depositing them in conventional silica capillaries, followed by tapering [21] or by tapering the silica capillary template first and then depositing the semiconductor. The latter approach is preferred due to the mismatch

#160359 - $15.00 USD
Received 21 Dec 2011; accepted 24 Jan 2012; published 3 Feb 2012

in the thermomechanical properties of Ge, Si and silica that could lead to interfacial cracking while tapering the array of waveguides in a silica matrix. For tapering the empty MOF silica templates, a fusion splicer (Ericsson 995FA) was employed. An electric arc was used to locally heat the region to be tapered, and the fiber was simultaneously pulled with uniform longitudinal force in opposite directions. For chemical fluid deposition in these tapered templates, a mixture of 2 MPa germane (GeH_4) and 33 MPa helium (He) was configured to flow through the pores. Under these reaction conditions, deposition occurs at a relatively low temperature of 300 ⁾C, producing hydrogenated amorphous germanium waveguides (Fig. 2(c), 2(d)). Tapered Si waveguides were deposited [24] under similar reaction conditions using silane (SiH_4), except that the MOF is heated to 400 ºC to produce hydrogenated amorphous silicon (Fig. 2(a), 2(b)).

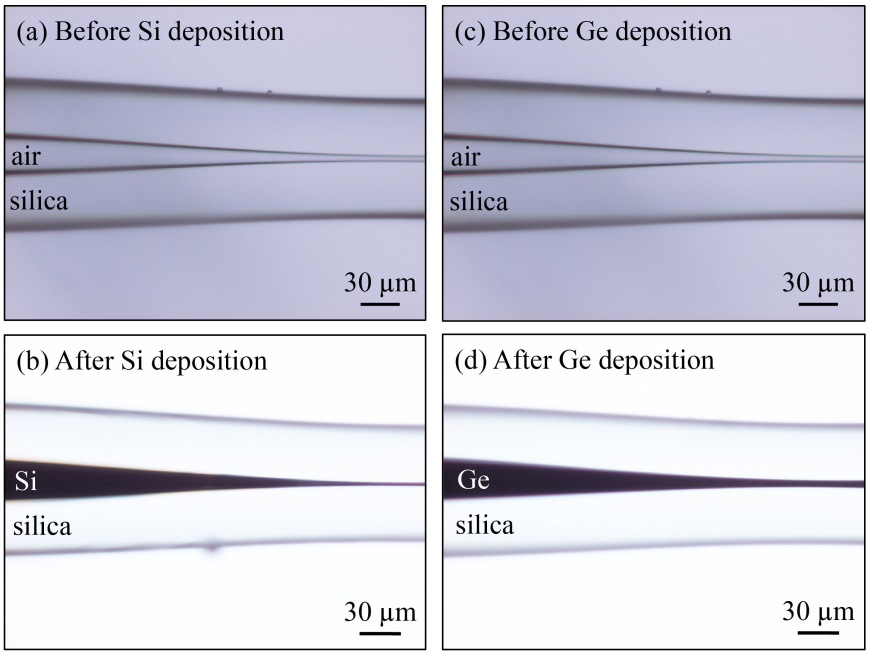

Fig. 2. Optical micrograph of a tapered silica capillary (a,c) before, and (b,d) after Si deposition (a,b), and Ge deposition (c,d).

Two taper structures are demonstrated, one based on Ge-filling and another based on Si-filling of holey silica fibers. Detailed specifications of each of these taper structures are given in Table 1. Optical micrographs of the input and output ends of the array of tapered waveguides after deposition are shown in Fig. 3. Note that the pixel magnification (ratio of wide to narrow end diameters of the pixels) is higher than the pitch magnification (ratio of wide to narrow end center-to-center distance between pixels), indicating a more aggressive taper of the waveguides as compared with the silica matrix. While the Ge is fully filled, Si filling demonstrated here has partial filling. This is due to the different reaction rates of silane and germane decomposition, and longer times and higher temperatures can result in fully filled Si regions as well [22–24]. However, these pixels will still guide light and function. For example, finite element method simulations indicate that a Si tube with a wall as thin as 50 nm inside a 2.5 µm silica capillary can still guide light and sustain at least 7 modes. This is demonstrated later in Fig. 4(d).

#160359 - $15.00 USD Received 21 Dec 2011; accepted 24 Jan 2012; published 3 Feb 2012

Table 1. Specifications of the Ge-Filled and Si-Filled Tapered Structures Fabricated in this Study

	Ge/SiO_2 taper	Si/SiO_2 taper
# Pixels	168	167
Length of taper	300 μm	300 μm
Taper outer diameter, narrow/wide ends	185/285 μm	195/260 μm
Pixel diameter at the narrow/wide ends	3.5-6/13 μm	2-2.5/9 μm
Pitch, narrow/wide ends	11.5/15 μm	9.5/13 μm
Pixel/pitch magnifications	2.2-3.7x/1.3x	3.6-4.5x/1.4x
Pixel cross-talk	11% at 10.64 μm	5% at 1.55 μm

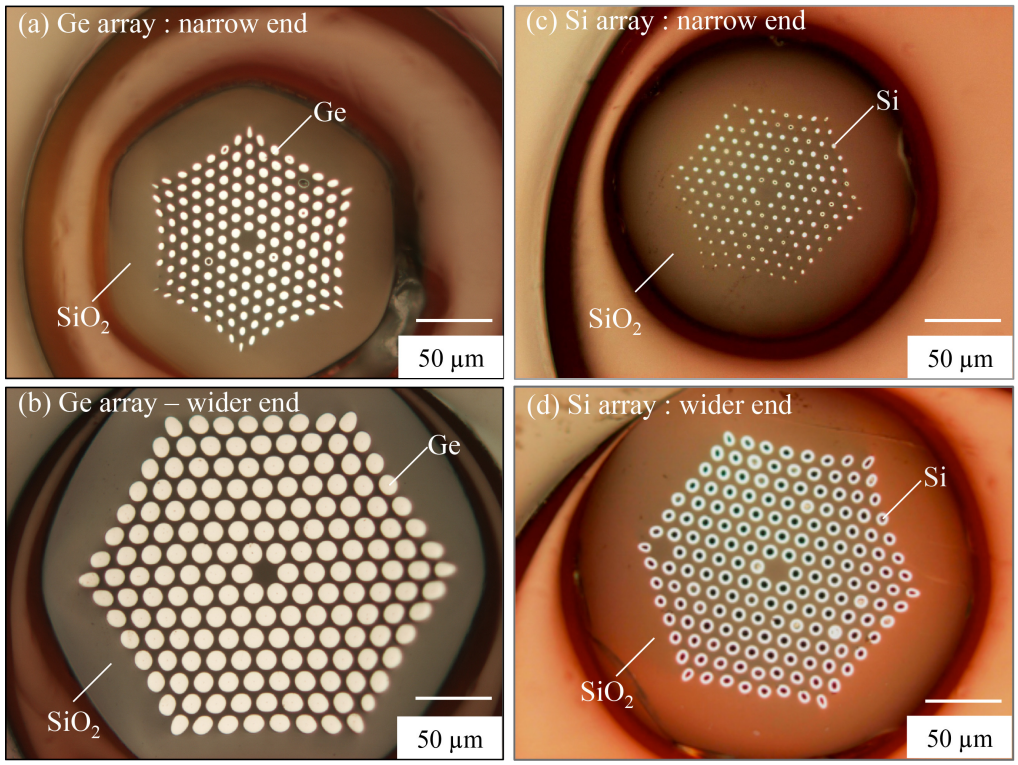

Fig. 3. Optical micrograph of the tapered array of Ge waveguides at the (a) narrow (input), and (b) wider (output) ends, and a tapered array of Si waveguides at the (c) narrow and (d) wide ends. Specifications are given in Table 1.

3. Image transfer with magnification

The inter-pixel cross-talk and image transfer and magnification capabilities of the tapered array of Ge and Si waveguides were characterized. The array was employed to transmit the magnified image of an object with sub-wavelength features. A metal mask representing the desired image was therefore fabricated at the input (narrow) end of the fiberscope as depicted in Figs. 4(a) and 4(c). To fabricate the mask, a uniform layer of 100 nm gold + 10 nm chromium (adhesion layer) was deposited on the input facet by an electron beam assisted evaporator. The metal layer covering the waveguides forming the letters 'P S U' (Ge taper) and an '↑' (Si taper) were selectively patterned in the metal layer by a focused ion beam (FIB) assisted milling technique (FEI Quanta 200 3D). Some pixels were thus exposed by milling, and the others remained masked by the metal layer.

#160359 - $15.00 USD
Received 21 Dec 2011; accepted 24 Jan 2012; published 3 Feb 2012

A continuous wave carbon-dioxide laser at 10.64 μm and a tunable laser at 1.55 μm were both used to uniformly illuminate the metal patterns on the Ge and Si fiberscopes, respectively. A 52x reflecting objective (Ealing) with 0.65 NA was used for collecting the magnified image transmitted through the tapered array of waveguides. The magnified image was focused onto a broadband camera. Under uniform illumination, the pixels in the 'P S U' pattern, and '↑' pattern at the input were magnified by 3x and 3.5x, respectively at the output plane. The intensity patterns recorded on the camera at 10.64 μm and 1.55 μm wavelengths are shown in Fig. 4(b), 4(d). The cross-talk and variation in the intensity profile of each of the exposed waveguide/pixel can be attributed to the variation in waveguide core diameters. The uniformity could be improved by further optimization of the processing conditions for deposition and tapering.

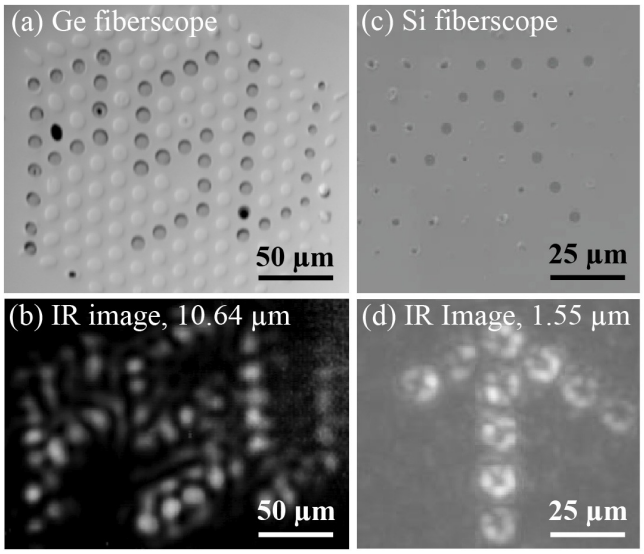

Fig. 4. Scanning electron micrographs of the metal mask exposing the pixels forming the pattern (a) 'P S U' and (c) '↑' at the tapered input end of the array of Ge and Si waveguides respectively. The intensity profile of the light transmitted through the (b) Ge and (d) Si fiberscope at 10.6 μm and 1.55 μm wavelengths, respectively.

In addition, numerical simulations of the fabricated structures based on finite element modeling (COMSOL™) under localized illumination were performed. The simulations indicate that a 2.5 μm diameter Si waveguide supports >90 modes at the wavelength of 1.55 μm, while a 3.5 μm diameter Ge waveguide supports ~6 modes at 10.6 μm wavelength. Hence they are highly multimode. The mode structure is not relevant to this imaging mode, since all one collects is the transmitted intensity of light in each pixel. As long as all pixels are identical, and transmit light, they will function as pixels. The cross-talk is defined as the ratio of the power measured at the output facet of a waveguide not illuminated but which is adjacent to an illuminated waveguide, to the power output from the illuminated waveguide. It was estimated by numerically integrating the power in the two regions from the simulated intensity profile and compared with the corresponding experimental cross-talk calculated from Figs. 4(b), 4(d). In the tapered Ge array, the experimentally measured cross-talk between pixels is found to be ~11% at 10.64 μm wavelength, in comparison to the 2% predicted by numerical modeling. In the tapered Si array, the experimentally measured cross-talk between pixels is found to be ~5% at 1.55 μm wavelength, in comparison to the 2% predicted by numerical modeling. After tapering the MOF template, the pore diameters were observed to decrease along the radius moving away from the center. This can be attributed to non-uniform temperature profile of silica during the tapering process. The process could be improved by

#160359 - $15.00 USD Received 21 Dec 2011; accepted 24 Jan 2012; published 3 Feb 2012

tapering the silica over longer time duration to achieve uniformity in the temperature distribution. The other source of cross-talk could be due to the imperfections occurring during the fabrication of the metal mask at the input. The *raw* optical throughput through the Ge array, defined as output power divided by the input power, without accounting for Fresnel reflection losses, was ~1.6×10^{-3}. Accounting for the reflection losses of ~36% each at the input and output Ge/air interfaces, and the fill factor of ~2 which is the ratio of the total area of pixels versus cladding at the mask, the actual power throughput is ~0.8%, which is excellent for a sub-wavelength probe.

4. Near-field scanning optical imaging

In order to demonstrate a near-field scan of the tip across an independent sample (Fig. 5(a)), a 16 μm inner diameter / 150 μm outer diameter empty glass fiber was tapered to a pinch using a fusion splicer, and then back-filled with a single core of Ge. The pinched end was polished back to where the Ge core has a 1.2 μm inner diameter; the broader end (16 μm diameter core) of the probe was also polished to optical quality. This fiber was mounted in a larger capillary with wax as shown in Fig. 5(b). The fiber was lightly etched with HF acid to expose the Ge core, and a 100 nm layer of gold was deposited on the narrow end of the taper. Finally, a focused ion beam was used to mill a 1 μm diameter aperture in the gold layer, concentric with the Ge core, shown in the inset of Fig. 5(b).

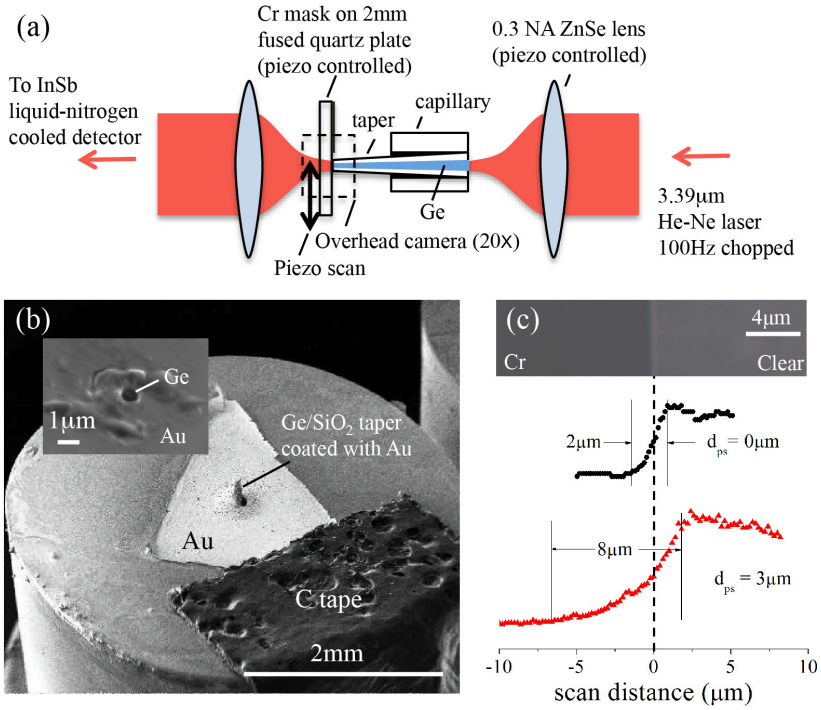

Fig. 5. (a) Schematic of a near-field scanning optical imaging setup. (b) Scanning electron micrograph of the tapered fiber with a ~1.2 μm Ge core (inset). (c) Conventional visible optical micrograph image of the mask (top), and the corresponding near-field infrared scan (bottom) of the Cr-edge in the nominal contact geometry (probe-sample distance, d_{ps}~0), and in non-contact geometry (d_{ps}~3μm).

Figure 5(a) shows a schematic diagram of the near-field measurement. The sample being imaged was a fused quartz plate with a chromium mask that is typically used in contact lithography (Fig. 5(c), top). A line scan was performed across a straight edge on the Cr-edge. The sample was brought in contact with the probe by piezoelectric actuators. No active

#160359 - $15.00 USD
Received 21 Dec 2011; accepted 24 Jan 2012; published 3 Feb 2012

feedback mechanism was employed for the approach. Instead, the fiber probe tip and its reflected image on the chromium mask were observed with an overhead camera. The sample was translated toward the probe until the probe and its image were in contact. Line scans across the chromium edge were performed at different probe-sample distances as shown in Fig. 5(c), bottom. The best resolution obtained was ~2 μm in contact geometry, which is larger than the probe aperture diameter. A possible reason for this might be a lack of true contact either due to the approach, or due to the lack of perfect flatness of the metal coating on the fiber tip, as shown in the inset of Fig. 5(b). The metal coating is shown to have a topography of ~0.5-1 μm near the core, which could have led to a finite d_{ps}, that is nominally marked as zero in Fig. 5(c). If one considers a high numerical aperture (NA) infrared objective of ~0.85, the diffraction limited spot size at 3.39 μm wavelength would be expected to be ~0.6l/NA = 2.4 μm in air. The demonstrated near-field resolution is slightly better than this. Thus, this experiment has demonstrated a sub-vacuum-wavelength, sub-diffraction limit imaging resolution, obtained in the near-field geometry. The *raw* optical throughput, defined as the light detected by the detector through the optical fiber taper in the geometry of Fig. 1(a), divided by the light detected with the same setup but without the fiber taper, and with the ZnSe lenses placed to focus and re-collimate in air, was measured to be $5x10^{-4}$. Accounting for the reflection losses of ~36% each at the two germanium-air interfaces at the input and output facets of the fiber tip, the tip throughput is roughly ~$4x10^{-3}$ or 0.4%, which is excellent.

5. Conclusions

In summary, we have demonstrated the proof-of-concept of infrared image magnification and transfer at sub-wavelength resolution and magnification using a tapered array of semiconductor waveguides. An image with a pixel size of 2-6 μm and a pitch size of 9.5-11.5 μm is transmitted with a built-in magnification of ~2.2-4.5x at wavelengths of 10.64 μm and 1.55 μm. Scanning near-field imaging is demonstrated with a sub-vacuum-wavelength resolution of ~2 μm. The resolution can be further improved by optimizing the parameters to aggressively taper the starting MOF template. Simulations indicate that the imaging system demonstrated can be used for various imaging applications anywhere in the broad transmission window of Ge between λ~2-15 μm and Si for λ~1.1-8 μm. The ability to deposit high index infrared transparent semiconductors such as Ge (n~4) and Si (n~3.5) inside silica matrix fibers (n~1.5) allows for the possibility of strong light confinement and large optical throughput imaging elements. The conceptual design can be extended to the visible wavelength regime by appropriate choice of materials for the waveguide core such as zinc selenide (ZnSe) [25]. For example, the cross-talk of ~5-11% could be further reduced by fabricating waveguides with a second cladding structure of ZnSe around the cores in order to reduce the extent of the mode in the silica glass. The next logical step would be to perform 2-dimensional near-field imaging of real samples with such fiber tips with an array of waveguides for interesting applications in optical data storage and near-field photolithography.

Acknowledgments

The authors acknowledge EPSRC (EP/G028273/1), NSF (DMR-0806860 and DMR-1107894), and the Penn State Materials Research Science and Engineering Center (DMR-0820404) for financial support.

#160359 - $15.00 USD Received 21 Dec 2011; accepted 24 Jan 2012; published 3 Feb 2012